**A Volcano Rekindled: The Renewed Eruption of Mount St. Helens, 2004–2006**
Edited by David R. Sherrod, William E. Scott, and Peter H. Stauffer
U.S. Geological Survey Professional Paper 1750, 2008

# Chapter 27

# Chlorine Degassing During the Lava Dome-Building Eruption of Mount St. Helens, 2004–2005

By Marie Edmonds[1], Kenneth A. McGee[2], and Michael P. Doukas[2]

## Abstract

Remote measurements of volcanic gases from the Mount St. Helens lava dome were carried out using Open-Path Fourier-Transform Infrared spectroscopy on August 31, 2005. Measurements were performed at a site ~1 km from the lava dome, which was used as a source of IR radiation. On average, during the period of measurement, the volcanic gas contained 99 mol percent $H_2O$, 0.78 percent $CO_2$, 0.095 percent HCl, 0.085 percent $SO_2$, 0.027 percent HF, $4.8\times10^{-4}$ percent CO, and $2.5\times10^{-4}$ percent COS close to the active vent. The fluxes of these species, constrained by synchronous measurements of $SO_2$ flux, were 7,200 t/d $H_2O$, 140 t/d $CO_2$, 22 t/d $SO_2$, 14 t/d HCl, 2.0 t/d HF, 54 kg/d CO, and 59 kg/d COS, ±20 percent. Observations of $H_2O$/Cl in the vapor and melt are compared to models of closed- and open-system degassing and to models where a closed system dominates to depths as shallow as ~1 km, and gases are then allowed to escape through a permeable bubble network. Although several features are consistent with this model—for example, (1) $H_2O$/Cl in the gases emitted from stagnant parts of the lava dome, (2) the concentration of Cl in the matrix glass of erupted dacite, and (3) the glass $H_2O$/Cl—the gases emitted from the active part of the lava dome have much higher $H_2O$/Cl than expected. These higher $H_2O$/Cl levels result from a combination of two factors (1) the addition of substantial amounts of ground water or glacier-derived $H_2O$ to the gases at shallow depths, such that only ~10 mol percent of the measured $H_2O$ is magmatic, and (or) (2) some Cl present as alkali chloride (NaCl and KCl) in the gas phase. The mean molar Cl/S is similar to gases measured at other silicic subduction-zone volcanoes during effusive activity; this may be due to the influence of Cl in the vapor on S solubility in the melt, which produces a solubility maximum for S at vapor Cl/S ~1.

## Introduction

Volcanic gases comprise water ($H_2O$), carbon dioxide ($CO_2$), sulfur dioxide ($SO_2$), hydrogen sulfide ($H_2S$), hydrogen chloride (HCl), and, to a lesser extent, hydrogen fluoride (HF), carbon monoxide (CO), and a host of trace species (for example, Symonds and others, 1994). Volatiles (mainly $H_2O$ and $CO_2$) exsolve from magma during decompression, generating vesicularity and buoyancy relative to the surrounding rocks, thereby driving eruptions. The rate and style of degassing controls the rheological development of magma and governs eruptive style (for example, Sparks and others, 2000). Preeruptive dissolved $H_2O$, $CO_2$, S, and Cl contents in silicic magmas typically range from 1 to 6 weight percent and 0–400, 30–200 and 900–3,000 ppm, respectively, after having undergone ~60–70 percent vapor-saturated fractional crystallization at 2–5 kb in the crust to evolve from mafic magma compositions (Wallace, 2005).

Chlorine is a significant volatile component of magmas associated with subduction zones and is derived from devolatilization of the subducting lithospheric slab (Manning, 2004). Recent analysis of volatile fluxes at subduction zones indicates that the flux of subducted Cl in the form of seawater and sediments approximately balances the output from arc volcanism (~$4–7\times10^{12}$ g/yr), consistent with the low abundance of Cl in mantle plume-derived basalt tapping the deep mantle (Wallace, 2005). Along with other volatiles, Cl dissolves in the partial melt and, thereafter, behaves as an incompatible element during crystallization, although small amounts may be taken up by amphibole phases. Cl is finally removed from the melt by partitioning into a vapor phase during magma ascent through the crust. A high partition coefficient (vapor/melt) for Cl was first recognized by Kilinc and Burnham (1972). The release

[1]U.S. Geological Survey, P.O. Box 51, Hawaii National Park, HI 96718; now at University of Cambridge, Downing Street, Cambridge CB2 3EQ, U.K.

[2] U.S. Geological Survey, 1300 SE Cardinal Court, Vancouver, WA 98683

of Cl with $H_2O$ and other volatiles from magma is important for the transport and concentration of ore metals, such as gold, copper, and iron, which may eventually form mineral deposits in large magmatic systems (Lowenstern and others, 1991). The acidic nature of HCl-containing gases may leach and alter volcanic rocks and contribute to instability in volcanic edifices (Le Friant and others, 2002).

Hydrogen chloride is the dominant chloride species in volcanic gases (Webster and Holloway, 1988); significant amounts of NaCl and KCl have also been detected (Le Guern and others, 1975). Gaseous HCl enters the atmosphere during volcanic eruptions; tropospheric emissions can cause local acid rain, and stratospheric injection of HCl gas can lead to degradation of the ozone layer (Tabazedeh and Turco, 1993). The rate of emission of HCl from volcanoes, compared to that of $SO_2$, has been linked to eruptive processes and has applications for volcano monitoring. Stoiber and Rose (1974) noted that gas Cl/S tends to increase throughout an eruptive episode, owing to the lower solubility of S. At Augustine Volcano, Symonds and others (1990) noted that older volcanic deposits exsolved gas with higher Cl/S than the main eruptive vents, suggesting that Cl continues to degas from melt after emplacement at the surface. At Soufrière Hills volcano[3], Montserrat, S-rich basaltic magma is supplied to the base of a porphyritic, Cl-rich andesite body. Volcanic gases with high levels of Cl/S are emitted during eruptive periods and gases with low levels of Cl/S are emitted during noneruptive periods. These emissions are caused by the degassing of negligible Cl but extensive S from the basalt to a vapor phase at 5–7 km; and the degassing of Cl but negligible S from the andesite during eruption (Edmonds and others, 2002).

During the current eruption of Mount St. Helens (ongoing in August 2006), $CO_2$, $SO_2$, and $H_2S$ emission rates have been measured regularly and are well constrained (Gerlach and others, this volume, chap. 26); $H_2O$, HCl, and other minor species had not been quantified until this study. HCl is an important constituent of volcanic gases, yet fewer measurements of HCl than of $SO_2$ are carried out during volcanic eruptions. This paper presents new data on the composition of the volcanic gas plume emitted from the lava dome at Mount St. Helens in August 2005. Remote spectroscopic measurements of the volcanic plume made by using Open-Path Fourier-Transform Infrared spectroscopy (OP–FTIR) yield the relative proportions of magmatic $H_2O$, $CO_2$, HCl, $SO_2$, HF, CO, and COS of the gas phase. Synchronous measurements of $SO_2$ emission rates are used to calculate emission rates for the other six species.

The emission of Cl in the form of HCl gas is the focus of the analysis. In order to interpret the rate and mechanism of HCl emission from volcanoes, an understanding of how magmatic vapor evolves chemically with changes in pressure, temperature, and melt composition is necessary; this is reasonably constrained for $H_2O$, $CO_2$, and $H_2O$-$CO_2$ melt-vapor systems at shallow to intermediate pressures (for example, for basaltic melts, Dixon and others, 1995) but less well understood for systems containing S and Cl. The measured molar $H_2O$/Cl of the gases is compared to models describing different degassing regimes in order to evaluate the evolution of the vapor phase with magma ascent. The gas composition is compared to the compositions of volcanic gases at other silicic volcanoes and to observations made during 1980–86 at Mount St. Helens. The Cl/S molar ratio is evaluated with reference to the solubility of S and Cl in silicic melts.

## Method

Open-path Fourier-transform infrared spectroscopy (OP–FTIR) is a spectroscopic technique that utilizes the absorptivity of specific gas molecules in order to quantify them accurately (fig. 1*A*). A spectrometer acquires infrared (IR) radiation from a source that has passed through volcanic gas. Di-atomic and monatomic compounds (for example, $H_2$, He) do not have an IR signature and, thus, cannot be measured by this technique. Absorption due to the gases is isolated and calibrated. OP–FTIR has been used successfully at several volcanoes, including Unzen, Japan (Mori and others, 1993); Vulcano, Italy (Francis and others, 1995); Etna, Italy (Burton and others, 2003); Soufrière Hills, Montserrat (Edmonds and others, 2002); and Kīlauea, USA (Edmonds and others, 2005). The OP–FTIR technique has advantages over direct methods of sampling, the most important of which is the remote aspect of the measurements and, hence, the higher level of safety, because it is not necessary to approach the fumaroles or vents closely. This technique is particularly useful for measuring gases at lava dome-building volcanoes, where explosions can occur with little warning; measurements can be collected throughout eruptive and noneruptive periods. For example, during the 1980–86 Mount St. Helens eruption, gas sampling was possible only from peripheral fumaroles, and when the lava dome was particularly active, no gas samples were collected at all (Gerlach and Casadevall, 1986). OP–FTIR also allows rapid measurements; several hundred spectra may be collected every hour, each containing information about the amount of various major and minor gas species in the pathlength.

The OP–FTIR data presented in this paper were collected on August 31, 2005, using the 2004–5 Mount St. Helens lava dome as a source of IR radiation (fig. 1). A digital elevation model formulated from photographs taken on September 1, 2005, (S.P. Schilling, written commun., 2008) is shown in figure 2. The massive parts of the dome were broken whaleback-shaped spines, each surrounded by a thick layer of blocky talus material. The measurements were taken in three sets; pathlengths ranged from 1,040 to 1,150 m (fig. 2). Temperatures on the surface of the lava dome were highly variable,

[3]Capitalization of "Volcano" indicates adoption of the word as part of the formal geographic name by the host country, as listed in the Geographic Names Information System, a database maintained by the U.S. Board on Geographic Names. Noncapitalized "volcano" is applied informally—eds.

ranging from ~10°C to >200°C (fig. 3). For the OP–FTIR measurements, cracks in the spine surfaces were used as IR sources and had temperatures as high as 600°C (Schneider and others, this volume, chap. 17). Volcanic gas rose from the lava dome (fig. 1*B*) and passed through the spectrometer's field of view.

A MIDAC IR spectrometer with a resolution of 0.5 $cm^{-1}$ was mounted onto a 20-inch Newtonian telescope on a heavy-weight tripod (fig. 1*A*). The spectrometer design incorporates a Michelson interferometer, laser optics, $CaF_2$ optical windows, and an InSb Stirling-cycle cooled detector with a range of 5,000–1,800 $cm^{-1}$. The field of view of the instrument is 2–3 m at 800 m. A laptop computer and PCMCIA interface enable real-time data acquisition and processing, using Autoquant4 software (MIDAC Corp.). Analysis is based on a linear model of the sample absorbance known as Beer's Law, which can be written as:

$$A_i = \sum_{j=1}^{M} a_{ij} LC_j \qquad i = 1, 2 \ldots N, \tag{1}$$

where $M$ is the number of compounds assumed to absorb in the spectral region analyzed; $A_i$ is the observed sample absorbance at the $i$th frequency, $C_j$ is the (unknown) concentration of the $j$th component of the mixture, $L$ is the absorption pathlength used in recording the sample spectrum and $a_{ij}$ is the absorptivity of the $j$th compound at the $i$th IR frequency. $A_i$, the absorbance spectrum, is obtained from the measured spectrum by normalizing the measured spectrum, $S_i$, by a background spectrum $B$, which is free of, or contains less, absorption due to volcanic gases:

$$A_i = -\log\left(S_i / B\right). \tag{2}$$

The absorbance spectra, therefore, contain information pertaining only to the volcanic gas phase; all other background gases are canceled out by this procedure. The absorbance spectra, $A_i$, are baseline corrected (in each fitting region) before analysis, using a second-order polynomial, and they also are corrected for their temperature and pressure relative to the reference spectra. A calibration set of spectra of pure components at known concentrations are used to calculate the absorptivities $a_{ij}$.

The uncertainty in the measurements is calculated from the residual spectrum, which should have a mean of zero in the fitted region and is proportional to the square root of the sum of the squares of the residual:

$$\sigma^2 = \sum_i R_i^2 \Big/ (n-1), \tag{3}$$

where $\sigma^2$ is the error variance, $R$ is the residual spectrum, and $n$ is the number of observations. The standard error of the estimated concentration, $\varepsilon$, is equal to:

$$\varepsilon = \sigma C \Big/ \sqrt{\sum_i A_i^2}. \tag{4}$$

This technique allows the evaluation of precise concentration-pathlengths ($LCj$ from equation 1) for each species, which have units of parts per million meters (ppm·m). The ratios of the concentration-pathlengths for different species in the plume typically are accurate to within a few percent, given appropriate analysis. The absolute values, however, are a minimum because the background spectrum, $B$, is not a clear-

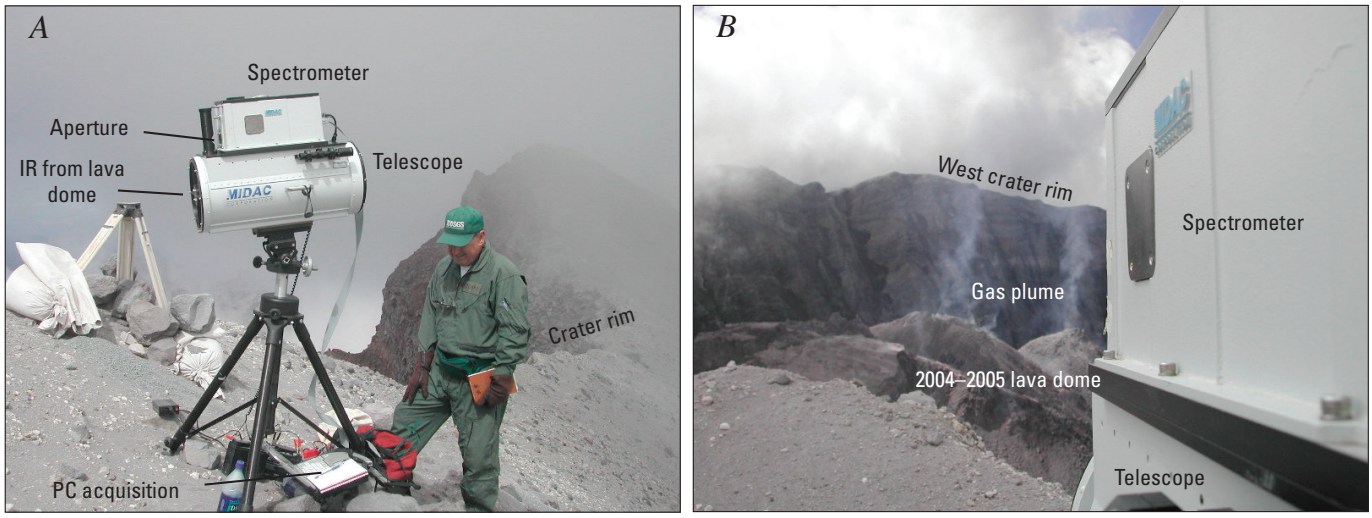


**Figure 1.** Fourier-transform infrared (FTIR) spectrometer in field settings. *A*, At FTIR measurement site (Brutus), on east crater rim of Mount St. Helens. *B*, Collecting radiation from hot cracks in the dacitic lava dome of Mount St. Helens, 2005. Volcanic gas is passing into the path in front of the infrared source.

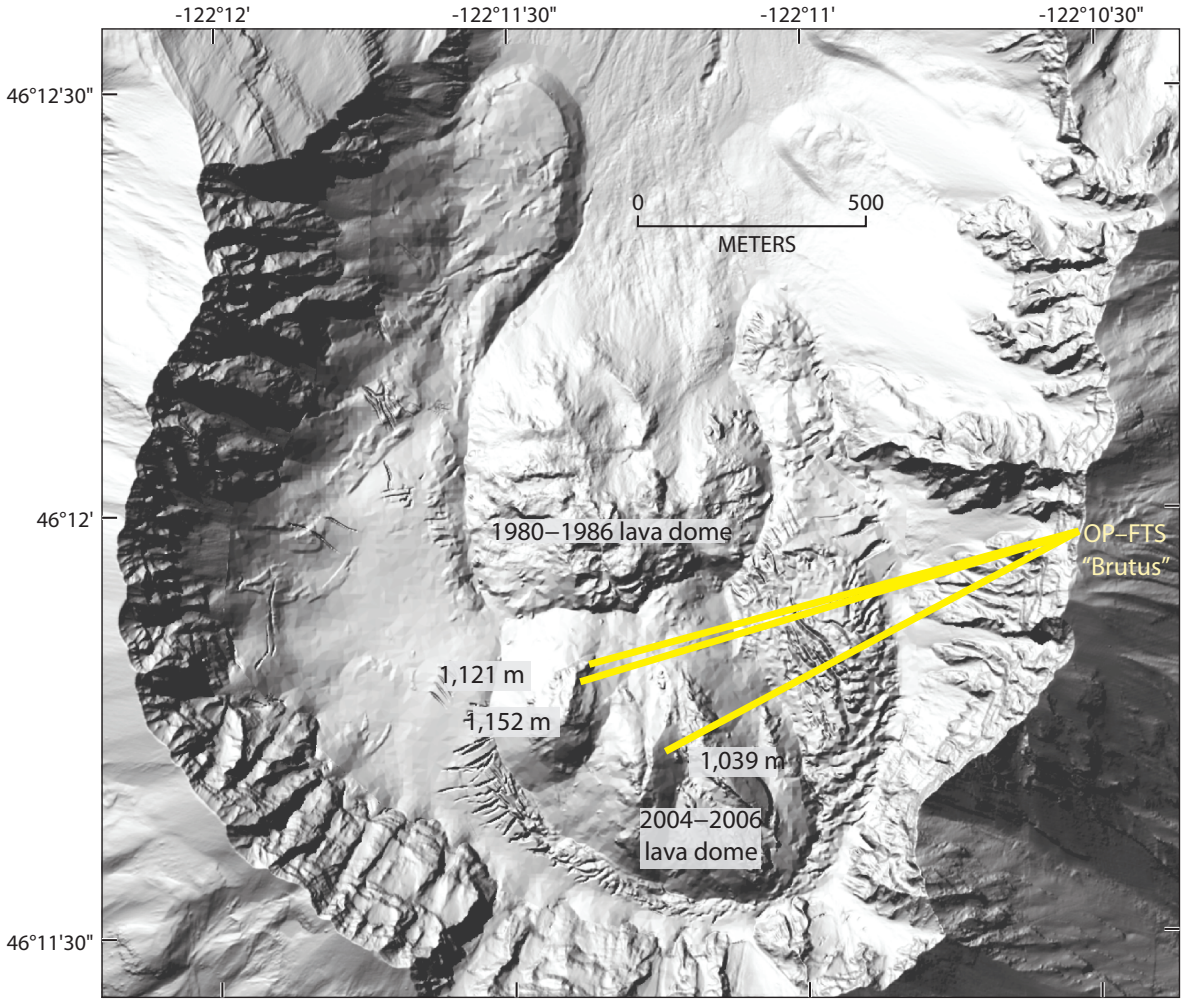


**Figure 2.** Shaded-relief digital elevation model of September 1, 2005, showing three paths used for OP–FTIR measurements in this study (courtesy of S.P. Schilling, USGS). Lengths of paths are labeled. Datum and projection are NAD83, UTM zone 10.

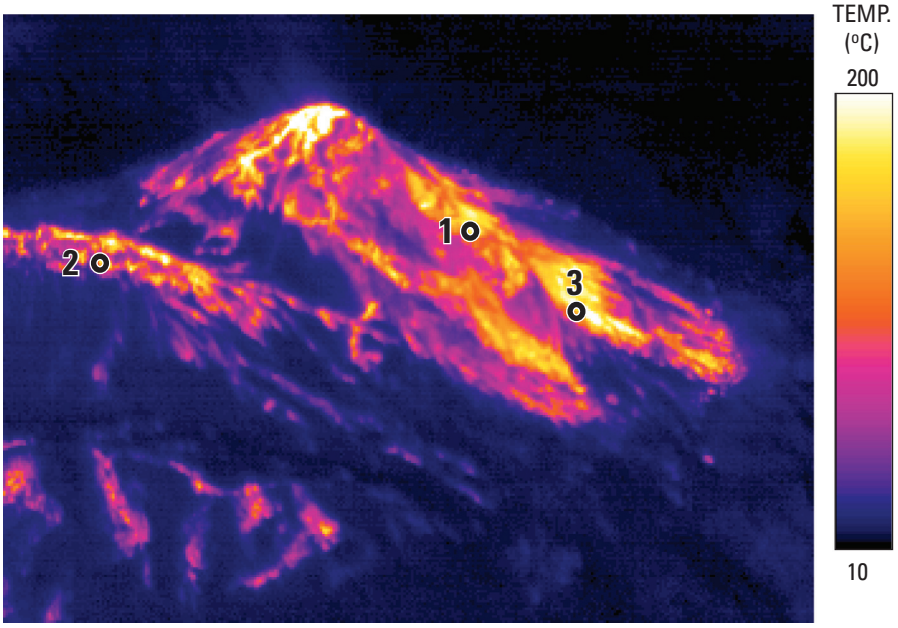


**Figure 3.** Thermal image, taken by forward-looking infrared radiometer (FLIR), showing lava dome from a helicopter near OP–FTIR measurement site (Brutus) on September 2, 2005 (courtesy of M. Logan, USGS). Numbers mark the parts of the lava dome used as infrared sources for measurement sets 1 to 3. Temperature scale on right.

**Table 1.** Summary of wavenumber windows used in analysis, detection limits, and mean errors for volcanic gas species detected by OP–FTIR in this study, Mount St. Helens, Washington, 2005.

| Species | Wavenumber window ($cm^{-1}$) | Detection limit (ppm·m) | Mean error (%) |
|---|---|---|---|
| $H_2O$ | 2134.80–2140.51 | 4,000 | 13.2 |
| $CO_2$ | 2264.26–2273.20 | 2,000 | 15.3 |
| HCl | 2744.18–2848.38 | 3 | 7.6 |
| $SO_2$ | 2447.36–2532.96 | 15 | 17.4 |
| HF | 4062.31–4089.16 | 20 | 14.1 |
| CO | 2089.29–2199.87 | 0.8 | 8.2 |
| COS | 2093.60–2020.87 | 0.7 | 7.6 |

sky spectrum for these measurements; rather, it is the spectrum containing the fewest molecules of volcanic gas in the series of measured spectra, $S_i$. A background spectrum under the exact conditions of the measurements containing no volcanic gas often is impossible to obtain in practice in this mode. Spectra were acquired once per second, and eight spectra were averaged, a procedure which typically took about 8 s.

In this study, retrievals for seven major volcanic gas species were carried out: $H_2O$, $CO_2$, HCl, $SO_2$, HF, CO, and COS. Retrievals for HCl and CO are relatively low in error, owing to their strong and fast absorption features; COS is detectable owing to its high absorptivity. Measured $SO_2$ exceeds detection limits, but the errors are larger owing to its weak absorption signature (at around 2,500 $cm^{-1}$). $H_2O$ has a moderately high error owing to its high and variable background concentration derived from nonmagmatic, highly variable local sources, such as evaporating ground water, ice, and meteoric water. At these long pathlengths, background $CO_2$ is around 280,000 ppm·m, and, in order to be detected, volcanic $CO_2$ must be present at levels >5 percent above background levels. The errors and detection limits on the measurements are shown in table 1.

The results of the measurements take the form of molar ratios and gas compositions. The molar ratios are calculated by plotting the abundance (in concentration-pathlength units) of one gas species against another. The gas species will plot in a straight line if they are derived from a common origin (the volcanic vent) and a gas of constant composition is being emitted. All background gases, including random amounts of nonvolcanic $H_2O$, are eliminated from the results, owing to the normalization by background spectra. Any mixing of the volcanic gas with ambient air should, therefore, not affect the results unless chemical reactions are taking place, or unless there is significant heterogeneity in the atmospheric air composition in the pathlength (which is significant here for $H_2O$). The mean slope of the plots of gas abundances is equal to the molar ratio between the two species. Changes in the concentration-pathlength of a species with time are controlled by source effects (variations in the emission rate of gases), combined with fluctuating wind speeds and directions, which blow the plume gases out of the pathlength. Pairs of species concentration-pathlengths are used to calculate molar ratios, thereby eliminating these source and wind effects, as they will affect all gases similarly.

Emission rates for $SO_2$ were measured by absorption spectroscopy with a miniature spectrometer manufactured by Ocean Optics and an instrumental housing (incorporating calibration cells; FLYSPEC) and software developed by Horton and others (2006). Horizontal traverses were made beneath the plume, approximately 1.5 km downwind of the lava dome. Integrated concentration-pathlength across the plume width was multiplied by the plume speed (measured by using methodology developed by Doukas, 2002) to generate $SO_2$ emission rates. Three measurements of $SO_2$ emission rates were carried out, and errors are less than 10 percent.

## Results

The spectra measured on August 31, 2005, record seven volcanic gas species: $H_2O$, $CO_2$, HCl, $SO_2$, HF, CO, and COS, in typical order of abundance for the three sets of measurements (fig. 2). The first set of measurements contained 109 spectra. The IR source for the measurements was part of spine 6, and the pathlength was 1,150 m (figs. 2, 3). These spectra recorded absorptions due to $H_2O$, HCl, CO, and COS gases; $CO_2$, $SO_2$, and HF were below detection, possibly due to a relatively low source temperature and (or) the long pathlength, both of which tend to decrease the signal-to-noise ratio. Figure 4 shows the characteristic absorption signature due to HCl gas in the measured spectra compared to a reference spectrum, the concentration-pathlength of $H_2O$ and HCl, and the concentration-pathlengths of CO and COS with time for this set of measurements. Table 2 shows a summary of the data (labeled set 1) and includes mean and maximum concentrations measured for each species and the mean $H_2O$/Cl ratio. The relatively low abundances of all the detected gases (HCl, as much as 147 ppm·m, and $H_2O$, as much as 21,000 ppm·m) suggest that the

abundances of $CO_2$ and $SO_2$ were probably below detection for this set of measurements. The mean $H_2O$/Cl molar ratio was 120 (table 2).

The second set of measurements were taken using a shorter pathlength of 1,040 m and a remnant of spine 5 as an IR source (figs. 2, 3). Figure 5 shows that HCl, HF, CO, and COS are detectable during the entire time period, whereas $H_2O$, $CO_2$, and $SO_2$ are detectable in only some of the spectra. Nondetection in some parts of the time series might be due to a weakening of the IR source or a decrease in gas-column abundance. The abundance of HCl ranged from 0 to 624 ppm·m over the pathlength, whereas $SO_2$ reached 251 ppm·m (table 2, set 2). Carbon monoxide reached a maximum concentration-pathlength of 15 ppm·m, and COS reached 2.6 ppm·m. The mean Cl/S ratio was 2.1, and $H_2O$/Cl was 85 (table 2).

The third set of measurements was taken using an IR source on spine 6, with a pathlength of 1,120 m (figs. 2, 3). This set of measurements imaged gases emitted from the

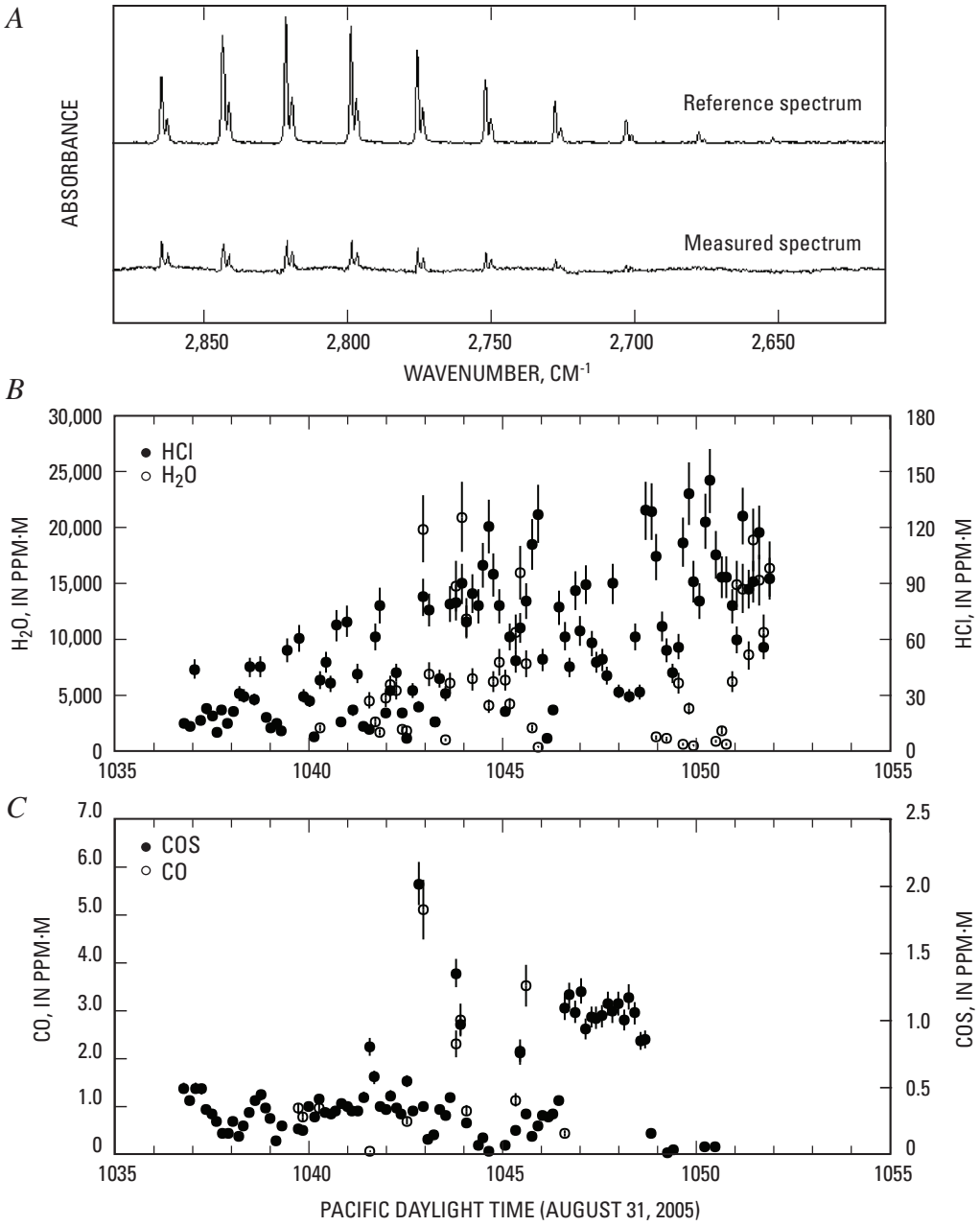


**Figure 4.** Data for measurement set 1, Mount St. Helens, Washington, 2005. *A*, Measured absorbance spectrum and reference spectrum for HCl gas for spectra collected along path 1. *B*, HCl and $H_2O$ concentration pathlengths. *C*, CO and COS concentration pathlengths with time for measurement set 1.

**Table 2.** Summary of OP–FTIR measurements (sets 1, 2, and 3), Mount St. Helens, Washington, 2005.

[$N$ is number of spectra in each set. Maximum $(LC)_{max}$ and mean $(LC)_{mean}$ are concentration pathlengths (in ppm·m) for the seven gas species detected; bd, below detection. Mean molar ratios are given with estimates of errors. Dashes show ratios not calculated where sulfur data are lacking.]

| Set | HCl | $SO_2$ | CO | $CO_2$ | COS | $H_2O$ | HF | Cl/S | Cl/F | $H_2O$/Cl | $SO_2$/COS | CO/$CO_2$ |
|---|---|---|---|---|---|---|---|---|---|---|---|---|
| 1 *N*=109 | | | | | | | | | | | | |
| $(LC)_{max}$ | 147 | bd | 5.1 | bd | 2.0 | 21,000 | bd | | | | | |
| $(LC)_{mean}$ | 57.0 | bd | 1.7 | bd | 0.47 | 7,000 | bd | -- | -- | 120±25 | -- | -- |
| 2 *N*=479 | | | | | | | | | | | | |
| $(LC)_{max}$ | 624 | 251 | 15 | 10,300 | 2.6 | 51,000 | 310 | | | | | |
| $(LC)_{mean}$ | 279 | 145 | 5.0 | 5,870 | 1.2 | 28,900 | 74 | 2.1±0.4 | 8.8±2.0 | 85±15 | 120±15 | 0.00086±0.0002 |
| 3 Active vent *N*=97 | | | | | | | | | | | | |
| $(LC)_{max}$ | 261 | 155 | 1.3 | 4,400 | 0.84 | 310,000 | 86 | | | | | |
| $(LC)_{mean}$ | 110 | 121 | 0.42 | 1,300 | 0.35 | 64,000 | 40 | 1.1±0.3 | 3.5±2.0 | 1040±200 | 350±60 | 0.00032±0.00006 |

area closest to the active vent at the base of the most recently erupted spine. $H_2O$, $CO_2$, HCl, $SO_2$, HF, CO, and COS were detected in the absorption spectra (fig. 6 and table 2). The abundances of the gases were generally less than for measurement set 2; HCl concentration pathlengths reached 261 ppm·m, and $SO_2$ reached 155 ppm·m (table 2, set 3). The mean molar $H_2O$/Cl was 1,040 and Cl/S was 1.1. The molar ratios can be used to formulate a gas composition (table 3, column A). The gas was composed mainly of $H_2O$ (99 mol percent), with 0.78 mol percent $CO_2$, 0.095 mol percent HCl, 0.085 mol percent $SO_2$, and minor amounts of HF, CO, and COS. For comparison, a gas sample collected in September 1981 (Gerlach and Casadevall, 1986) is shown in column D. Columns B and E show the same gas compositions recalculated to $H_2O$-free compositions, and columns C and F show them recalculated to $H_2O$- and $CO_2$-free compositions. The gas composition measured in 2005 is similar to that measured in 1981, albeit with less CO and more COS.

The ultraviolet spectrometer traverses carried out at 1400 PDT on August 31, 2005, yielded a mean $SO_2$ flux of 22 t/d. By converting the molar gas composition into the mass composition (table 4) for measurement set 3, the $SO_2$ emission rate (bold, table 4) can be used to calculate emission rates for the six other species. On August 31, 2005, $H_2O$ was emitted at rates of about 83 kg/s (7,200 t/d), $CO_2$ at 1.6 kg/s (140 t/d), HCl at 0.16 kg/s (14 t/d), and HF at 0.024 kg/s (2.0 t/d). CO and COS were emitted at rates of 0.63 and 0.69 g/s, respectively; these fluxes are associated with errors of ~±20 percent. $CO_2$ emission rates were measured independently by using LICOR and were found to be 198 t/d (Gerlach and others, this volume, chap. 26). The excess can be attributed to a small amount of $CO_2$ degassing from the 1980–86 lava dome (Gerlach and others, this volume, chap. 26), which was not captured by the OP–FTIR measurements.

# Discussion

## Partitioning of Cl into Aqueous Vapor

Experimental work on Cl behavior in silicic magmas demonstrates the strong affinity that Cl has for a $H_2O$-rich vapor phase (Kilinc and Burnham, 1972; Webster and Holloway, 1988). The fluid-melt partition coefficient increases with decreasing temperature and with increasing dissolved melt Cl content; and decreases with decreasing pressure (Shinohara and others, 1989), although the latter is not well constrained. The partition coefficient is high for subaluminous melts and decreases with increasing aluminous or peralkaline character (Webster, 1992). Increasing the Cl molality of the vapor phase to high levels causes the formation of an immiscible Cl-rich liquid, as observed in the $H_2O$-NaCl system (Shinohara and others, 1989). Signorelli and Carroll (2002) determined Cl solubility limits of 4,800–6,800 ppm for the hydrous rhyolite melt of recent Soufrière Hills volcano eruptions, which has a (Na+K)/Al ~0.6. These concentrations are much higher than those observed in melt-inclusion glasses (Edmonds and others,

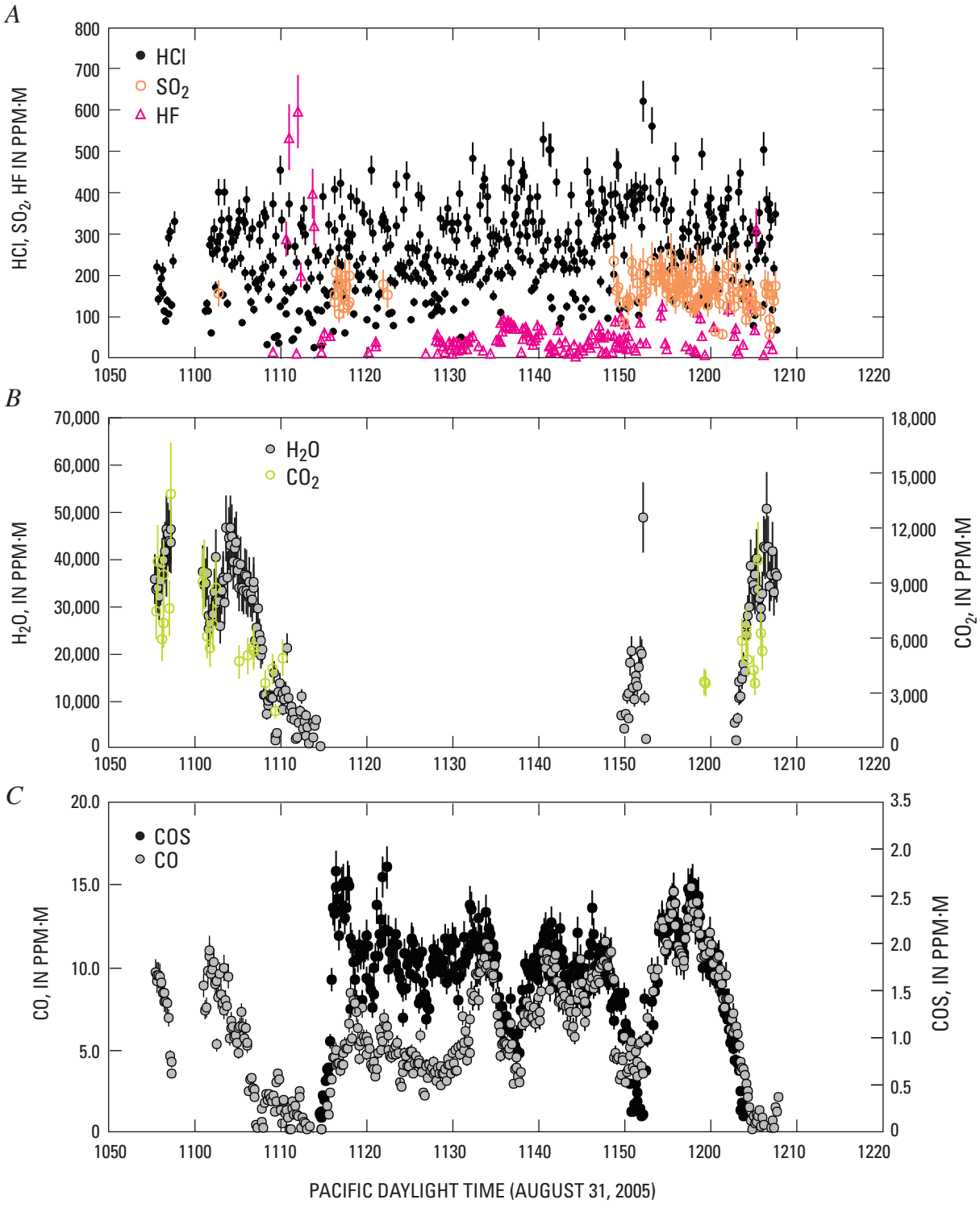


**Figure 5.** Data for measurement set 2, Mount St. Helens, Washington, 2005, as concentration pathlengths with time. *A*, HCl, HF, and $SO_2$. *B*, $H_2O$ and $CO_2$. *C*, CO and COS.

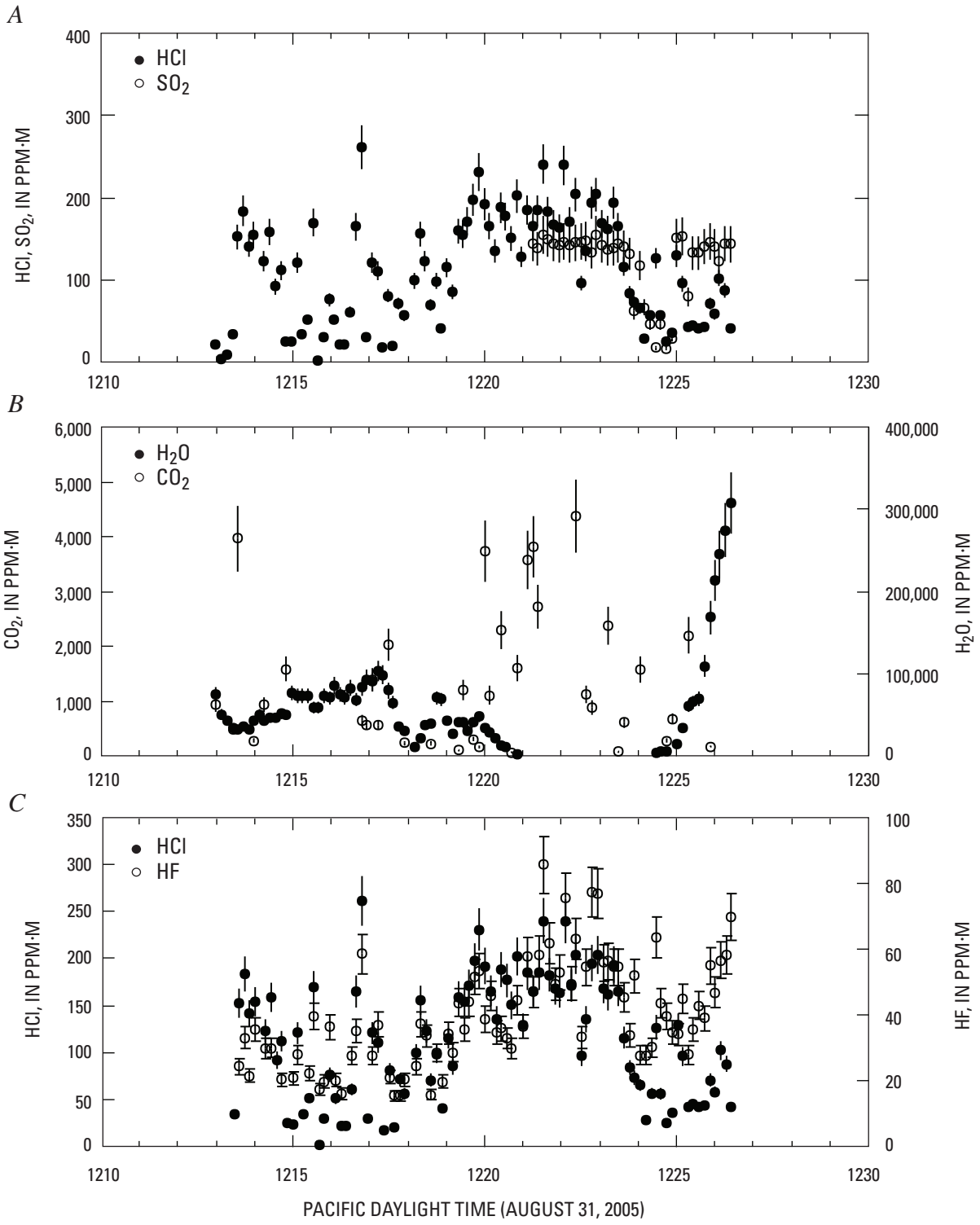


**Figure 6.** Data for measurement set 3, Mount St. Helens, Washington, 2005, as concentration pathlengths with time. *A*, HCl and $SO_2$. *B*, $H_2O$ and $CO_2$. *C*, HCl and HF.

**Table 3.** Gas compositions at Mount St. Helens, 1981 and 2005.

[Compositions (in molar percent) derived from this study (column A) are compared with a representative gas composition derived from sampling of gases by using caustic soda in May 1981 (column D; Gerlach and Casadevall, 1986). Columns B and E show the gas compositions recalculated to $H_2O$-free compositions. Columns C and F show the gas compositions recalculated to $H_2O$- and $CO_2$-free compositions.]

| | This study (set 3) | | | September 17, 1981 | | |
|---|---|---|---|---|---|---|
| | A | B | C | D | E | F |
| $H_2O$ | 99 | | | 99 | | |
| $CO_2$ | 0.78 | 79 | | 0.89 | 83 | |
| HCl | 0.095 | 9.7 | 46 | 0.076 | 7.2 | 43 |
| $SO_2$ | 0.085 | 8.6 | 41 | 0.067 | 6.3 | 38 |
| HF | 0.027 | 2.8 | 13 | 0.030 | 2.8 | 17 |
| CO | 0.00048 | 0.049 | 0.23 | 0.0023 | 0.22 | 1.3 |
| COS | 0.00025 | 0.025 | 0.12 | $1.8\times10^{-5}$ | 0.0017 | 0.010 |

**Table 4.** Gas composition derived from this study (from measurement set 3), Mount St. Helens, Washington, 2005, in molar percent and mass percent.

[Flux of each species is calculated using the flux of $SO_2$ gas measured with ultraviolet spectrometers (22 t/d; in bold). Fluxes expressed both in kg/s and in t/d.]

| Species | Molar % | Mass % | Flux (kg/s) | Flux (t/d) |
|---|---|---|---|---|
| $H_2O$ | 99 | 98 | 83 | 7,200 |
| $CO_2$ | 0.78 | 1.9 | 1.6 | 140 |
| HCl | 0.095 | 0.19 | 0.16 | 14 |
| $SO_2$ | 0.085 | 0.30 | 0.25 | **22** |
| HF | 0.027 | 0.028 | 0.024 | 2.0 |
| CO | 0.00048 | 0.00073 | 0.00063 | 0.054 |
| COS | 0.00025 | 0.00080 | 0.00069 | 0.059 |

2002) and suggest that the aqueous vapor phase was relatively Cl poor. In the case of Mount St. Helens, melt-inclusion data for the erupted products of 1980–86 indicate that the maximum Cl content of the preeruptive melt was around 1,000 ppm (Rutherford and others, 1985), which is within the range of Cl concentrations in melt inclusions from the 2004–5 eruption of Mount St. Helens (Pallister and others, this volume, chap. 30) and is much lower than the solubility for Cl in a melt with (Na+K)/Al ~1 at 850–900°C and 200 MPa (around 2,000–2,500 ppm; Metrich and Rutherford, 1992). If the 2004–5 Mount St. Helens melt had an initial $H_2O$ content of ~4.6 weight percent, similar to that obtained from melt-inclusion analysis for the 1980s erupted products (Rutherford and others, 1985), and if $P_{total}$ is equal to $P_{H_2O}$, then the melt was in equilibrium with a $H_2O$-rich vapor at a depth of around 6 km (assuming lithostatic pressure with depth). The preeruption dissolved Cl content of the melt at about 6 km is assumed to be close to 1,000 ppm, on the basis of the maximum Cl concentration measured in melt inclusions (Pallister and others, this volume, chap. 30), which is within range of typical silicic arc magmas (Wallace, 2005).

The $H_2O$/HCl molar ratio of the vapor varies during melt ascent and eruption and is controlled by water solubility and degassing, partitioning of Cl into the vapor, the degassing regime (whether open- or closed-system degassing or some combination of the two is in operation), and microlite crystallization on ascent (which will tend to increase the concentration of volatiles in the melt and promote further degassing). These factors can be incorporated into models describing the evolution of the vapor phase on ascent and compared with the

observations presented here. This analysis assumes there is no breakdown of hydrous phases (for example, amphibole), which would tend to increase the bulk $H_2O$ of the system on magma ascent.

Closed-system degassing occurs when volatiles exsolve and remain in contact and in equilibrium with the host melt. The vesicularity of the melt is related to the amount of volatiles exsolved and the total pressure. Closed-system degassing can occur (1) during rapid ascent of magma from depth, resulting in fragmentation when the overpressure inside the expanding bubbles exceeds the strength of the magma, (2) in static magma bodies as a result of second boiling, and (3) during slow ascent of magma at depths of greater than a few kilometers, where gas fractions will typically be too low for fragmentation to occur. The partitioning of Cl between melt and aqueous vapor can be used to describe closed-system degassing:

$$\left(X^0_{H_2O} - X_{H_2O}\right) = \left(\frac{X^0_{Cl}}{X_{Cl}} - 1\right) \Big/ D_{Cl}^{fluid-melt}, \quad (5)$$

where $X^0_{H_2O}$ and $X^0_{Cl}$ are the original $H_2O$ and Cl mass fractions, $X_{H_2O}$ and $X_{Cl}$ are the melt $H_2O$ and Cl mass fractions, and $D_{Cl}^{fluid-melt}$ is the vapor-melt coefficient for Cl (assumed here to be constant). $X_{H_2O}$ varies with pressure according to its solubility, which is calculated using VolatileCalc for a rhyolite melt at 920°C and with a $X^0_{H_2O}$ of 4.6 weight percent (Newman and Lowenstern, 2002).

Open-system degassing involves increments of vapor being removed from the host melt after exsolution. For volatiles that partition strongly into a vapor phase, this style of degassing results in efficient removal of the species from the melt. This style of degassing may occur (1) along conduit sidewalls, where exsolved volatiles can escape by migrating upward or through the conduit walls, or (2) during shallow, slow ascent of magma, when sufficient porosity develops to allow permeability and vapor escape through a three-dimensional bubble network (for example, Blower, 2001); significant gas loss through bubble ascent would be suppressed by the high viscosity of the magma and crystals. Open-system degassing can be modeled using a Rayleigh fractionation equation (for example, Villemant and Boudon, 1999):

$$X_{Cl} = X^0_{Cl} f^{\alpha}, \quad (6)$$

$$\text{where } \alpha = \left(D_{Cl}^{fluid-melt} - 1\right), \quad (7)$$

$$\text{and } f = 1 - \left[\left(X^0_{H_2O} - X_{H_2O}\right) \Big/ X^0_{H_2O}\right], \quad (8)$$

where $f$ is the fraction of water remaining in the melt. $X_{Cl}$ is calculated for 5-MPa increments in pressure and converted to depth (km) assuming lithostatic pressures and a mean crustal density of 2,500 kg/m$^3$.

In order to account for microlite crystallization on ascent, which decreases the melt volume and causes increased exsolution of water, a factor $q$ was introduced to the equation for the open-system degassing case, whereby

$$q = q^0 - q^0\left(\left(X^0_{H_2O} - X_{H_2O}\right) \Big/ X^0_{H_2O}\right), \quad (9)$$

where $q^0$ is the initial melt fraction (taken to be 0.6). The expression for $f$, the fraction of $H_2O$ remaining in the melt, is modified thus:

$$f = 1 - \left[\left(X^0_{H_2O} - X_{H_2O}\right) \Big/ X^0_{H_2O}\right] - \left[\left(\frac{q_n}{q_{n-1}}\right) X_{H_2O} - X_{H_2O}\right], \quad (10)$$

where $q_n$ is the melt fraction for the previous step and $q_{n-1}$ is the melt fraction for the current step and $q_{n-1} < q_n$. This has the effect of decreasing $f$ to a slightly greater degree at each step to account for the effects of microphenocryst and microlite crystallization.

Figure 7 shows the results for closed- and open-system degassing for three partition coefficients ($D$). These results show the large dependence of the vapor composition at the surface on degassing regime. The plots show the depletion of Cl in the melt, the ratio of dissolved $H_2O$/Cl, and the $H_2O$/Cl ratio in the vapor phase, with depth. Three measured parameters are marked on the plots to compare to the model data: (1) the mass fraction of dissolved Cl, (2) the $H_2O$/Cl in the matrix glass of the erupted products (for microcrystalline and flow-banded dacite; from Pallister and others, this volume, chap. 30; summarized in table 5), and (3) the mass ratio $H_2O$/Cl in the volcanic gases (converted from molar ratios given in table 2). The $H_2O$/Cl in gases from measurement sets 1 and 2 range from 35 to 70 and are labeled stagnant dome (SD), and those from measurement set 3 range from 430 to 630 and are labeled active dome (AD).

The mass fraction of Cl in the melt, dissolved melt $H_2O$/Cl, and vapor $H_2O$/Cl from the stagnant dome are consistent with closed-system degassing, with a large partition coefficient ($D$~50) for Cl, from depths of ~ 6 km. The active dome gases are richer in $H_2O$ and are closer to the modeled $H_2O$/Cl for an open-system degassing regime. Open-system degassing from depth would deplete the melt almost entirely of Cl, however, which is not the case (figs. 7*A*, *B*); open-system degassing from depth is therefore inconsistent with observation. Closed-system degassing from depth with constant $D$ is consistent with observation but unrealistic on two counts: (1) closed-system degassing could not physically lead to lava dome building, owing to the inevitably large gas fractions that would result at shallow depths, and (2) a constant partition coefficient for Cl is improbable, based on the experiments of Shinohara and others (1989), which suggests that $D$ is strongly dependent on both dissolved melt Cl and on pressure.

Recent studies of degassing during the lava dome building of Soufrière Hills volcano, Montserrat, have shown that the degassing of $H_2O$ in the upper conduit leads to cooling,

crystallization, and an increase in viscosity of the magma (for example, Sparks and others, 2000). The development of permeability during degassing in the top ~1 km of the conduit leads to gas loss and effusive eruption. In order to investigate whether this mechanism is consistent with the proportions of $H_2O$ and Cl in the melt and in volcanic gases at Mount St. Helens, the model is adjusted by using equation 5 in order to incorporate the effects of closed-system degassing at depths greater than 1 km with the same mean fluid-melt partition coefficients for Cl (3, 10, and 50), followed by open-system degassing along the top 1 km of the conduit (fig. 8), using equations 6–10 with fluid-melt partition coefficients of 1, 2, and 3 ( $X^0_{H_2O}$ and $X^0{}_{Cl}$ are set equal to the final $X_{H_2O}$ and $X_{Cl}$ given by the closed-system degassing model at 1-km depth; fig. 8). A partition coefficient of 1 represents the case whereby no further degassing of Cl occurs. The plots in figures 7 and 8 are, therefore, identical up to 1-km depth; at shallower depths, the effects of open-system degassing are shown in figure 8. Observations of the melt and gases are marked on figure 8 to compare to the models. The mass fraction of Cl remaining dissolved in the melt, the melt $H_2O$/Cl, and the $H_2O$/Cl for gases emitted from the stagnant part of the lava dome are consistent with deep, closed-system degassing ($D$~10), followed by open-system degassing with $D$~2–3 (fig. 8). A decrease in $D$ to <5 was noted by Shinohara and others (1989) for lithostatic pressures corresponding to depths less than 2 km.

**Table 5.** Mean concentrations of Cl and $H_2O$ in erupted matrix glasses of microcrystalline (from 5 measurements) and flow-banded (from 12 measurements) dacite, Mount St. Helens, Washington, 2004—2005.

[From Pallister and others, this volume, chap. 30.]

| Matrix glass | Cl (ppm) | $H_2O$ (wt%) | $H_2O$/Cl |
|---|---|---|---|
| **Microcrystalline dacite** | | | |
| Mean concentration | 278 | 1.40 | 41 |
| 1σ deviation | 53 | 0.98 | 24 |
| **Flow-banded dacite** | | | |
| Mean concentration | 853 | 2.40 | 28 |
| 1σ deviation | 47 | 0.29 | 4.5 |

The $H_2O$/Cl of gases emitted from the active part of the lava dome, however, are not consistent with any of the theoretical models formulated here. This may be due to one or all of three factors: (1) a cessation of Cl degassing in the top 1 km of the conduit, (2) addition of substantial amounts of meteoric, ground-water, and glacier-derived $H_2O$ to the gases at shallow

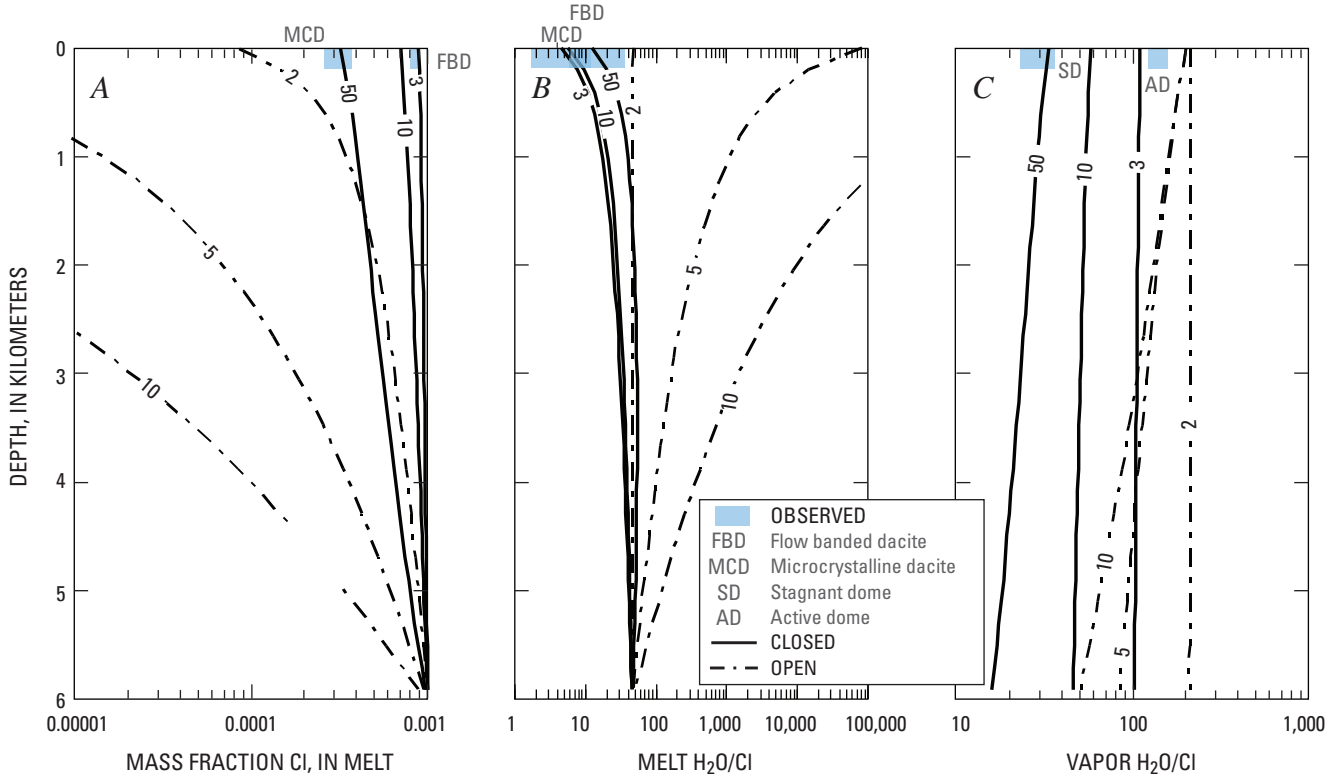


**Figure 7.** Effect on evolution of gases with depth for various models of degassing regime. Solid lines indicate closed-system degassing models and are labeled with the fluid-melt partition coefficient, D. Dot-dash lines indicate open-system degassing models and are labeled with the fluid-melt partition coefficient. Blue boxes indicate observed melt Cl, melt $H_2O$/Cl, and vapor $H_2O$/Cl. *A*, Fraction of Cl in melt. *B*, Dissolved melt $H_2O$/Cl. *C*, vapor $H_2O$/Cl.

depths, or (3) some Cl present as alkali chloride (NaCl and KCl) in the gas phase, as observed by Le Guern and Shinohara (1985) and studied experimentally by Shinohara and others (1989). The proportions of dissolved $H_2O$ and Cl remaining in the erupted glasses suggests that there is no cessation of Cl degassing in the top 1 km of the conduit (fig. 8; compare observations to solid line presenting $D$=1), so this factor is discounted. Shevenell and Goff (1999) used oxygen- and hydrogen-isotope data from hot springs to show that only 30–70 mol percent of the $H_2O$ in the fumaroles around the lava dome in 1981–86 was magmatic. In this case, the discrepancy between models and observations requires that only ~10 mol percent of the measured $H_2O$ be magmatic. Modification of the gas composition is shown in table 3, column A; using this factor yields 91 mol percent $H_2O$ and 7 mol percent $CO_2$, which might be more representative of the magmatic gas composition. The presence of alkali chlorides in the gas phase is consistent with the presence of chloride encrustations on the lava dome (possibly halite and (or) sylvite) observed during 2004–5 (C.R. Thornber, oral comm. 2005). Yellow encrustations on the September 1980 lava dome were noncrystalline and composed of Al, Cl, Fe, Ca, S, and $H_2O$. A sublimate film near fumaroles <250°C produced a yellow-brown stain on crack walls, which had a high Cl content (Keith and others, 1981).

## Comparison and Significance of Molar Cl/S

The behavior of S in silicic melts differs significantly from both Cl and $H_2O$. The partitioning of sulfur into a vapor phase is controlled by several factors, the most significant being the fugacities of oxygen and sulfur in the vapor phase and melt composition (Carroll and Webster, 1994). The solubility of sulfur is much lower than that of Cl for a given set of magmatic conditions. Table 6 shows molar Cl/S measured using a variety of techniques during eruptions at a range of dacitic and andesitic subduction-zone volcanoes, including the 1980–86 Mount St. Helens lava-dome eruption. The molar ratio measured during this study is similar (within error) to ratios measured at most other volcanoes and to ratios measured during the 1980–86 Mount St. Helens eruption, with the notable exception of Soufrière Hills volcano, which shows considerably higher Cl/S during lava dome-building activity. A molar Cl/S of ~1 appears to be a dominant feature of most reported gas compositions measured during eruptions in subduction-zone settings.

Botcharnikov and others (2004) reported solubility data for melts coexisting with mixed $H_2O$-Cl-S gases to illustrate the effect of multiple volatile components on their solubility. The total Cl content of the melt-vapor system can affect the

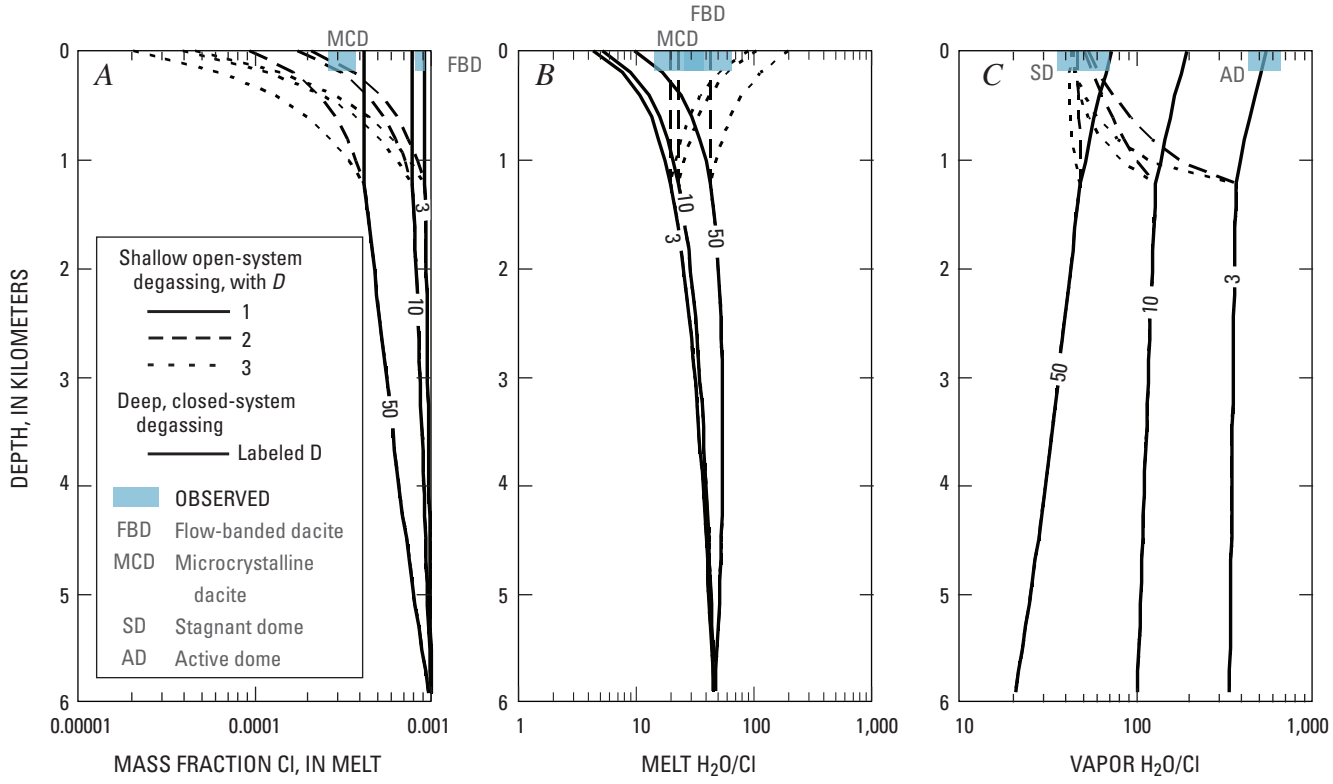


**Figure 8.** Effect of closed, then open-system (in the upper 1 km of the conduit) degassing on the composition of volcanic gases at the surface. The evolution of (*A*) the fraction of Cl in the melt, (*B*) dissolved melt $H_2O$/Cl, and (*C*) vapor $H_2O$/Cl with depth (km) for various models of degassing regime are shown. Closed-system degassing regimes are indicated by solid lines up to 1 km depth, labeled with values of D. Above 1 km depth, open-system degassing regimes are shown as dashed-dotted lines for three different values of D (see key). Observed melt Cl, melt $H_2O$/Cl, and vapor $H_2O$/Cl are shown as blue boxes.

**Table 6.** Molar Cl/S ratios in volcanic gases measured at other silicic subduction-zone volcanoes and at Mount St. Helens, Washington, 2005.

[Errors are estimated as ranging from 5 to 10 percent. OP–FTIR, open-path Fourier-transform IR spectroscopy; EBS, evacuated bottle sampling.]

| Volcano | Type | Method | Cl/S |
|---|---|---|---|
| Usu-san, Japan[1] | Basaltic andesite | OP–FTIR | 0.8 |
| Mount St. Helens, USA[2] | Dacite | EBS | 1.2 |
| Mount St. Helens, USA[3] | Dacite | OP–FTIR | 1.1 |
| Augustine Volcano, USA[4] | Dacite | EBS | 1.0 |
| Unzen-dake, Japan[5] | Dacite | OP–FTIR | 0.9 |
| Soufrière Hills, Montserrat[6] | Andesite | OP–FTIR | 2.0 |

[1]Mori and others, 1997.

[2]Gerlach and Casadevall, 1986.

[3]This study.

[4]Symonds and others, 1990.

[5]Mori and others, 1993.

[6]Edmonds and others, 2002.

solubility of S (Botcharnikov and others, 2004). The addition of 1 weight percent Cl increased S solubility by two times at 850°C and 200 MPa for a dacite-composition melt, with all other conditions constant. For a given $H_2O$ vapor concentration, over a range of total S content and solubility, a maximum S solubility occurred corresponding to a vapor Cl/S of ~1. A vapor Cl/S of ~1 may, therefore, be a direct consequence of the presence of moderate amounts of Cl in the melt, which is typical for arc magmas; vapor Cl/S might further be buffered by the addition or depletion of small amounts of Cl to the system. The maximum in S solubility might be explained by two main factors (Botcharnikov and others, 2004): (1) S is dissolved as sulphate ($SO_4^{2-}$) in hydrous melts, where oxygen fugacity is relatively high, and as sulfide ($S^{2-}$) at low oxygen fugacities (Carroll and Webster, 1994); the transition occurs at oxygen fugacities close to NNO. The addition of Cl to an S-bearing system might shift the redox conditions to slightly more oxidized conditions. The other possibility is (2) that S-Cl-bearing complexes may form in the melt, which would increase the solubilities of both components.

## The Abundance of Minor Gaseous Components (HF, CO, COS)

The solubility of fluorine (F) in silicic melts is generally much higher than that of Cl and, hence, does not degas to the same extent (Carroll and Webster, 1994). The vapor-melt partition coefficient for F is usually less than unity (Webster, 1990). Table 2 shows that the molar ratio of Cl/F in the volcanic gases is around 3.5. A similar molar Cl/F has been reported at a number of other silicic volcanoes in subduction-zone settings (Symonds and others, 1994) and compares well with the abundance of HF emitted from fumaroles at Mount St. Helens in September 1981 (table 3; Gerlach and Casadevall, 1986).

The mean $CO/CO_2$ ratio of the gases of around $3.2\times10^{-4}$ (table 2) implies that the gases equilibrated at a temperature of about 570°C, on the basis of the relation:

$$\log\left(CO/CO_2\right) = 1.76 - 4417/T, \qquad (11)$$

where $T$ is the temperature in Kelvin (Mori and Notsu, 1997). Collection temperatures derived from similar relations in gases sampled in 1981 ranged from 620°C to 762°C (Gerlach and Casadevall, 1986).

COS has been detected previously in volcanic plumes (for example, Le Guern and others, 1975), although measurements are few. Rasmussen and others (1982) reported abundances of 5 ppm by volume in the Mount St Helens gas plume of May 18, 1980, and suggested that injection of COS contributes to the stratospheric S burden during large silicic eruptions. Gerlach and Casadevall (1986) report molar $SO_2$/COS of 2,000 to 4,750 for gas samples collected at Mount St Helens from May to September 1981 from radial fumaroles around the lava dome. The mean molar ratios obtained August 31, 2005, using OP–FTIR are much lower than they were in the earlier samples, 350 (table 2, set 3) and 120 (set 2). Mori and Notsu (1997) reported $SO_2$ / COS of 400 for gases emitted from a fumarole at Aso, Japan, at a temperature of ~740°C.

## Conclusions

Several conclusions can be drawn from the results and interpretation presented here:

- The fluxes of magmatic volatiles from Mount St. Helens on August 31, 2005, were 7,200 t/d $H_2O$, 140 t/d $CO_2$, 14 t/d HCl, 22 t/d $SO_2$, 2.0 t/d HF, 54 kg/d CO, and 59 kg/d COS.
- The $H_2O$/Cl ratio in the gases emitted from stagnant parts of the Mount St Helens lava dome, and the amount of Cl and the $H_2O$/Cl in the erupted glasses in the melt, are all consistent with a model of closed-system degassing up to ~ 1-km depth (with a fluid-melt partition coefficient, *D*, for Cl of ~10), followed by open-system degassing to the surface (with a *D* of ~2–3). This is similar to models proposed for lava dome-building eruptions elsewhere, where much of the gas loss occurs in the upper 1 km of the conduit, causing cooling, crystallization, and an increase in magma viscosity.
- The gases emitted from the active part of the Mount St Helens lava dome have an $H_2O$/Cl that is about one order of magnitude higher than that predicted for closed- or open-system degassing or the two-stage model above. This is explained by as much as 90 mol percent of the measured $H_2O$ vapor being nonmagmatic (ground- or glacier-derived) and by some of the Cl being present as alkali chlorides in the gas phase (NaCl and KCl).
- Molar Cl/S in the gases measured in August 2005 is similar to that measured during 1980–86 at Mount St. Helens and at silicic subduction-zone volcanoes elsewhere during similar styles of eruption. This similarity may be caused by a maximum in S solubility when vapor Cl/S ~1, which is valid for the typical range in initial S and Cl (100–300 and 1,000–3,000 ppm, respectively) at silicic subduction-zone volcanoes.
- The gas analyses presented here confirm that remote spectroscopic techniques are capable of measuring the composition of high-temperature gases remotely and safely during lava dome building at silicic volcanoes, provided the measurements can be made using a pathlength ≤1 km with sufficient gas molecules in the path to enable detection. There is scope for automated measurements with more compact instruments that consume less power, enabling the development of time series and further analysis of the degassing regime throughout an eruption.

## Acknowledgments

This work was done with the support of the USGS Mendenhall Postdoctoral Fellowship Program and the Center for the Study of Active Volcanoes (CSAV) at the University of Hawai`i, Hilo. Michelle Coombs and Jacob Lowenstern provided detailed and thorough reviews, which improved the manuscript enormously.

## References Cited

Blower, J.D., 2001, Factors controlling permeability-porosity relationships in magma: Bulletin of Volcanology, v. 63, no. 7, p. 497–504.

Botcharnikov, R.E., Behrens, H., Holtz, F., Koepke, J., and Sato, H., 2004, Sulfur and chlorine solubility in Mt. Unzen rhyodacitic melt at 850°C and 200 MPa: Chemical Geology, v. 213, no. 1–3, p. 207–225.

Burton, M.R., Allard, P., Mure, F., and Oppenheimer, C., 2003, FTIR remote sensing of fractional magma degassing at Mount Etna, Sicily: Geological Society Special Publication, v. 213, p. 281–293.

Carroll, M.R., and Webster, J.D., 1994, Solubilities of sulfur, noble gases, nitrogen, chlorine and fluorine in magmas: Reviews in Mineralogy, v. 30, p. 231–280.

Dixon, J.E., Stolper, E.M., and Holloway, J.R., 1995, An experimental study of water and carbon dioxide solubilities in mid-ocean ridge basaltic liquids; Part I, Calibration and solubility models: Journal of Petrology, v. 36, no. 6, p. 1607–1631.

Doukas, M.P., 2002, A new method for GPS-based wind speed determinations during airborne volcanic plume measurements: U.S. Geological Survey Open-File Report 02–395, 13 p.

Edmonds, M., Pyle, D.M., and Oppenheimer, C., 2002, *HCl* emissions at Soufrière Hills Volcano, Montserrat, West Indies, during a second phase of dome building, November 1999 to September 2000: Bulletin of Volcanology, v. 64, p. 21–30.

Edmonds, M., Gerlach, T.M., Herd, R.A., Sutton, A.J., and Elias, T., 2005, The composition of volcanic gas issuing from Pu‘u ‘Ō‘ō, Kīlauea Volcano, Hawai‘i, 2004–5 [abs.]: Eos (American Geophysical Union Transactions), v. 86, no. 52, San Francisco, December 5–9, 2005. Fall Meet. Suppl. Abstract, V13G–08.

Francis, P.W., Maciejewski, A., and Oppenheimer, C., 1995, $SO_2$/HCl ratios in the plumes from Mt. Etna and Vulcano determined by Fourier transform spectroscopy: Geophysical Research Letters, v. 22, p. 1717–1720.

Gerlach, T.M., and Casadevall, T.J., 1986, Evaluation of gas data from high-temperature fumaroles at Mount St. Helens, 1980–1982: Journal of Volcanology and Geothermal Research, v. 28, nos. 1–2, p. 107–140, doi:10.1016/0377-0273(86)90008-9.

Gerlach, T.M., McGee, K.A., and Doukas, M.P., 2008, Emission rates of $CO_2$, $SO_2$, and $H_2S$, scrubbing, and preeruption excess volatiles at Mount St. Helens, 2004–2005, chap. 26 *of* Sherrod, D.R., Scott, W.E., and Stauffer, P.H., eds., A volcano rekindled; the renewed eruption of Mount St. Helens, 2004–2006: U.S. Geological Survey Professional Paper 1750 (this volume).

Horton, K.A., William-Jones, G., Garbeil, H., Elias, T., Sutton, A.J., Mouginis-Mark, P., Porter, J.N., and Clegg, S., 2006, Real-time measurement of volcanic $SO_2$ emissions—validation of a new UV correlation spectrometer (FLYSPEC): Bulletin of Volcanology, v. 68, no. 4, p. 323–327, doi:10.1007/s00445-005-0014-9.

Keith, T.E.C., Casadevall, T.J., and Johnston, D.A., 1981, Fumarole encrustations—occurrence, mineralogy and chemistry, *in* Lipman, P.W., and Mullineaux, D.R., eds., The 1980 eruptions of Mount St. Helens, Washington: U.S. Geological Survey Professional Paper 1250, p. 239–250.

Kilinc, I.A., and Burnham, C.W., 1972, Partitioning of chloride between a silicate melt and coexisting aqueous phase from 2 to 8 kilobars: Economic Geology, v. 67, p. 231–235.

Le Friant, A., Boudon, G., Komorowski, J.-C., and Deplus, C., 2002. The island of Dominica, site for the generation of the most voluminous debris avalanches in the Lesser Antilles: Comptes Rendus Geoscience, v. 334, no. 4, p. 235–243, doi:10.1016/S1631-0713(02)01742-X.

Le Guern, F., and Shinohara, H., 1985, Etna 1983 composition of the magmatic gases [abs.]: International Association of Volcanology and Chemistry of the Earth's Interior, General Assembly 1985, Giardini-Naxos, Italy, abstract vol. no. QE272 I58 A2 1985.

Le Guern, F., Giggenbach, W., and Tazieff, H., 1975, Equilibres chemiques des gaz eruptifs du volcan Erta`Ale (Ethiopie): Comptes Rendus Hebdominaires des Seances de l'Aacademie des Sciences, Serie D: Sciences naturelles, v. 280, p. 2093–2095.

Lowenstern, J.B., Mahood, G.A., Rivers, M.L., and Sutton, S.R., 1991, Evidence for extreme partitioning of copper into a magmatic vapor phase: Science, v. 252, p. 1405–1409.

Manning, C., 2004. The chemistry of subduction-zone fluids: Earth and Planetary Science Letters, v. 223, p. 1–16.

Metrich, N., and Rutherford, M.J., 1992, Experimental study of chlorine behavior in hydrous silicic melts: Geochimica et Cosmochimica Acta, v. 56, p. 607–616.

Mori, T., and Notsu, K., 1997, Remote CO, COS, $CO_2$, $SO_2$, HCl detection and temperature estimation of volcanic gas: Geophysical Research Letters, v. 24, no. 16, p. 2047–2050.

Mori, T., Notsu, K., Tohjima, Y., and Wakita, H., 1993, Remote detection of HCl and $SO_2$ in volcanic gas from Unzen Volcano, Japan: Geophysical Research Letters, v. 20, no. 13, p. 1355–1358.

Newman, S., and Lowenstern, J.B., 2002, VolatileCalc—a silicate melt-$H_2O$-$CO_2$ solution model written in Visual Basic for excel®: Computers and Geosciences, v. 28, no. 5, p. 597–604, doi:10.1016/S0098-3004(01)00081-4.

Pallister, J.S., Thornber, C.R., Cashman, K.V., Clynne, M.A., Lowers, H.A., Mandeville, C.W., Brownfield, I.K., and Meeker, G.P., 2008, Petrology of the 2004–2006 Mount St. Helens lava dome—implications for magmatic plumbing and eruption triggering, chap. 30 *of* Sherrod, D.R., Scott, W.E., and Stauffer, P.H., eds., A volcano rekindled; the renewed eruption of Mount St. Helens, 2004–2006: U.S. Geological Survey Professional Paper 1750 (this volume).

Rasmussen, R.A., Khalil, M.A.K., Dalluge, R.W., Penkett, S.A., and Jones, B., 1982, Carbonyl sulfide and carbon disulfide from the eruptions of Mount St. Helens: Science, v. 215, p. 665–667.

Rutherford, M.J., Sigurdsson, H., Carey, S., and Davis, A., 1985, The May 18, 1980 eruption of Mount St. Helens—1. Melt composition and experimental phase equilibria: Journal of Geophysical Research, v. 90, no. B4, p. 2929–2947.

Shevenell, L., and Goff, F., 1999, Addition of magmatic volatiles into the hot spring waters of Loowit Canyon, Mount St. Helens, Washington, USA: Bulletin of Volcanology, v. 55, no. 7, p. 489–503, doi:10.1007/BF00304592.

Shinohara, H., Iiyama, J.T., and Matsuo, S., 1989, Partition of chlorine compounds between silicate melt and hydrothermal solutions—1. Partition of NaCl-KCl: Geochimica et Cosmochimica Acta, v. 53, p. 2617–2630.

Signorelli, S., and Carroll, M.R., 2002, Experimental constraints on the origin of chlorine emissions at the Soufriere Hills Volcano, Montserrat: Bulletin of Volcanology, v. 62, p. 431–440.

Sparks, R.S.J., Murphy, M.D., Lejeune, A.M., Watts, R.B., Barclay, J., and Young, S.R., 2000, Control on the emplacement of the andesite lava dome of the Soufrière Hills Volcano, Montserrat, by degassing-induced crystallization: Terra Nova, v. 12, no. 1, p. 14–20.

Stoiber, R.E., and Rose, W.I., 1974, Cl, F, and $SO_2$ in Central American volcanic gases: Bulletin Volcanologique, v. 37, no. 3, p. 454–460.

Symonds, R.B., Rose, W.I., Gerlach, T.M., Briggs, P.H., and Harmon, R.S., 1990, Evaluation of gases, condensates, and

$SO_2$ emissions from Augustine Volcano, Alaska—the degassing of a Cl-rich volcanic system: Bulletin of Volcanology: v. 52, p. 355–374.

Symonds, R.B., Rose, W.I., Bluth, G.J.S., and Gerlach, T.M., 1994, Volcanic-gas studies—methods, results and applications: Reviews in Mineralogy, v. 30, p. 1–66.

Tabazedeh, A., and Turco, R.P., 1993, Stratospheric chlorine injection by volcanic eruptions; HCl scavenging and implications for ozone: Science, v. 260, no. 5111, p. 1082–1086.

Villemant, B., and Boudon, G., 1999, $H_2O$ and halogen (F, Cl, Br) behaviour during shallow magma degassing processes: Earth and Planetary Sciences, v. 168, p. 271–286.

Wallace, P.J., 2005, Volatiles in subduction-zone magmas—concentrations and fluxes based on melt inclusion and volcanic gas data: Journal of Volcanology and Geothermal Research, v. 140, nos. 1–4, p. 217–240, doi:10.1016/j.jvolgeores.2004.07.023.

Webster, J.D., 1990, Partitioning of F between $H_2O$ and $CO_2$ fluids and topaz rhyolite melt—implications for mineralizing magmatic-hydrothermal fluids in F-rich granitic system: Contributions to Mineralogy and Petrology, v. 104, p. 424–438.

Webster, J.D., 1992, Water solubility and Cl partitioning in Cl-rich granitic system; effects of melt composition at 2 kbar and 800°C: Geochimica et Cosmochimica Acta, v. 56, p. 679–687.

Webster, J.D., and Holloway, J.R., 1988, Experimental constraints on the partitioning of Cl between topaz rhyolite melt and $H_2O$ and $H_2O$+$CO_2$ fluids—new implications for granitic differentiation and ore deposition: Geochimica et Cosmochimica Acta, v. 52, p. 2091–2105.